Syntheses, Characterization, and Hg(II) Adsorption Properties of Porous Cross-Linked Polystyrene Modified with 2-Aminopyridine via a Sulfoxide/Sulfone-Containing Spacer Arm†

Rongjun Qu,* Changmei Sun, Ying Zhang, Jian Chen, Chunhua Wang, Chunnuan Ji, and Xiguang Liu

School of Chemistry and Materials Science, Ludong University, Yantai 264025, China

Two chelating resins, porous cross-linked polystyrene modified with 2-amino-pyridine via a sulfoxide/sulfone-containing spacer (PVBSO-AP and $PVBSO_2$-AP), were synthesized. Their structures were characterized by a Fourier transform infrared spectrometer (FTIR), scanning electron microscopy (SEM), porous structure analysis, and elementary analysis. The results of SEM and pore analysis demonstrated that the two kinds of chelating resins maintained meso−macro porous structures. Some factors affecting the adsorption of Hg(II) on PVBSO-AP and $PVBSO_2$-AP resins such as contact time, solution concentration, and pH were investigated. The results showed that the optimum pH ranges appeared at (4.0 to 5.0) for PVBSO-AP and at (3.0 to 6.0) for $PVBSO_2$-AP resin, and the times reaching equilibrium were (8 and 5) h for the two resins, respectively. The experimental equilibrium data of Hg(II) onto the two resins showed that linear Langmuir and nonlinear Redlich−Peterson isotherms were the best fitting isotherms to describe the experimental data. The selectivity of adsorption of Hg(II) on PVBSO-AP and $PVBSO_2$-AP resins for Hg(II) were investigated in the binary ion systems. The results showed that the two resins can adsorb selectively Hg(II) in the presence of Ni(II), Zn(II), and Pb(II), and three adsorption−desorption cycles demonstrated that the two resins are suitable for reuse without considerable changes in the adsorption capacity.

1. Introduction

As everyone knows, mercury is highly toxic to living organisms. Commonly, mercury is used in a wide variety of industries such as electrical, paints, chlor-alkali, and pharmaceutical, and so forth. A number of approaches, such as reduction, precipitation, ion exchange, reverse osmosis, adsorption, and coagulation, have been suggested for the removal of mercury from aqueous solutions. Among these methods, selective adsorption of chelating resins is found to be very effective for the removal of mercury.[1−6]

Chelating resins with nitrogen-containing functional groups exhibit excellent adsorption selectivity for divalent transition metal ions due to the strong affinity between the nitrogen atom and these metal ions.[7−9] Aminopyridine, which contains two forms of N atoms, is found to exhibit high affinity and good adsorption selectivity for mercury.[10] Meanwhile, it has been proven that resins containing sulfur have an excellent selectivity of adsorption of Hg(II) and noble metals such as gold, silver, palladium, platinum, and so forth, owing to the low-lying empty 3d orbitals of sulfur.[4]

In the past decade, many efforts have been devoted to find the chelating resins to remove mercury from aqueous media.[11−18] Recently, we have designed and synthesized a series of novel chelating resins containing sulfur and nitrogen atoms. Their adsorption properties for metal ions were investigated systematically.[19−21] In our previous study, an interesting phenomenon was found that the sulfide bond in the chelating resins can be easily oxidized into sulfoxide or sulfone by certain oxidizing metal ions such as mercury(II) and gold(III).[15,22] The further study revealed that the oxide (sulfoxide or sulfone) chealting resins exhibited better adsorption selectivity than its counterpart sulfide chelating resin.[23] To investigate the synergetic effect between sulfoxide and aminopyridine in adsorption, we designed and synthesized a novel chelating resin containing sulfoxide and 3-aminopyridine via a sulfoxide-containing spacer arm, but the adsorption capacity is not important. The highest capacity of adsorption of Hg(II) was 0.65 $mmol \cdot g^{-1}$.[24] Hence, we also designed a novel chelating resin (PVBSO-AP) containing sulfoxide and 2-aminopyridine (AP) via a sulfoxide-containing spacer arm for further study. Meanwhile, as a reference resin, $PVBSO_2$-AP which contains a sulfone group was synthesized to compare the function of sulfoxide in PVBSO-AP resin. The structures of the two resins were characterized by a Fourier transform infrared spectrometer (FTIR), scanning electron microscopy (SEM), porous structure analysis, and elementary analysis, and their adsorption properties for Hg(II) were also investigated.

2. Experimental Section

2.1. Instruments and Reagents. Infrared spectra were recorded on a Nicolet MAGNA-IR 550 (series II) spectrophotometer (Nicolet, Japan); test conditions were as follows: potassium bromide pellets, scanning 32 times, resolution of 4 cm^{-1}. The data were treated with Thermo Nicolet Corporation OMNIC32 software of version 6.0a. The shapes and surface morphology of the resins were examined on a scanning electron microscope, JSF5600LV (JEOL, Japan). The concentration of metal ions was measured on a GBC-932 atomic absorption spectrophotometer (AAS) made in Australia by a cold AAS method. Test conditions were as follows: wavelength 253.7 nm, slit 0.7 nm, lamp current 3.0 mA, standard substance $HgCl_2$, and reducing agent, potassium borohydride. Porous structures of the resins were characterized using an automatic physisorption analyzer ASAP 2020 (Micromeritics

† Part of the "Sir John S. Rowlinson Festschrift".

* Corresponding author. Rongjun Qu. Tel.: +86 535 6699201. E-mail address: (rongjunqu@sohu.com or qurongjun@eyou.com).

10.1021/je100506d
Published on Web 09/24/2010

Scheme 1. Ideal Synthetic Routes of PVBSO-AP and $PVBSO_2$-AP

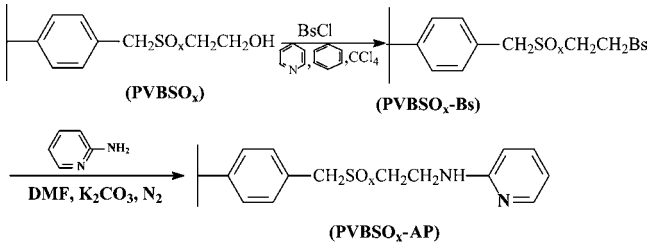

x=1, PVBSO-AP; x=2, $PVBSO_2$-AP

Instrument Corp., USA) by Brunauer−Emmett−Teller (BET) and Barrett−Joyner−Halenda (BJH) methods through N_2 adsorption at 77 K.

Poly[4-vinylbenzyl(2-hydroxyethyl)sulfoxide] (PVBSO) and poly[4-vinylbenzyl(2-hydroxyethyl)sulfone] ($PVBSO_2$) resins were prepared and characterized according to our previous work;[23] the contents of functional groups of −SO− and $-SO_2-$ are (3.90 and 3.79) mmol·g^{-1}, respectively. AP was purchased from The Academy of Military Medical (China) and used as received. Benzene sulfonyl chloride (BsCl) (Tingxin Chemical Factory, Shanghai, China) and the other reagents and solvents were reagent grade and were used without further purification.

2.2. Synthesis of PVBSO-AP and $PVBSO_2$-AP Resins. The PVBSO-AP and $PVBSO_2$-AP resins were prepared as described in Scheme 1.

A portion of 4.33 g of PVBSO resin was added into 85 mL of pyridine and swollen for 2 h in a three-necked flask. Then 8.1 mL of benzene sulfonyl chloride was added dropwise into the mixture under the condition of ice−water bath on the condition of mechanical stirring. The reaction was continued for 24 h at 18 °C. The spherical product was filtered off, washed with 20 mL of distilled water and 20 mL of ethanol, and then transferred to a Soxhlet's extraction apparatus for reflux-extraction in 95 % ethanol for 4 h. After dried under vacuum at 50 °C for 48 h, the resin PVBSO-Bs was obtained. Elemental analysis (%): S, 12.10.

Under the protection of nitrogen gas, 4.57 g of PVBSO-Bs (ca. 8.97 mmol $phSO_3-$) resin were swollen sufficiently in 80 mL DMF in a three-neck flask for more than 2 h, and then 3.22 g (ca. 34.30 mmol) of 2-amino pyridine and 1.58 g of K_2CO_3 (ca. 11.37 mmol) powder were added. With magnetic stirring, the mixture was reacted for 24 h at 120 °C. After cooling, the polymeric beads PVBSO-AP were filtered off and washed with dilute hydrochloric acid, dilute sodium hydroxide, distilled water, ethanol, acetone, and finally with methanol. The product PVBSO-AP was transferred to Soxhlet's extraction apparatus for reflux-extraction in 95 % ethanol for 10 h and then was dried under vacuum at 50 °C over 48 h. Elemental analysis (%): N, 1.927; S, 11.20.

A portion of 5.28 g of $PVBSO_2$ was swollen in 85 mL of pyridine for 2 h in a three-necked flask. Then, with mechanical stirring, 10.2 mL of benzene sulfonyl chloride was added dropwise into the mixture under the condition of ice−water bath. The reaction was continued for 24 h at 18 °C. The spherical product was filtered off, washed with 20 mL of distilled water and 20 mL of ethanol, and then transferred to a Soxhlet's extraction apparatus for reflux-extraction in 95 % ethanol for 4 h. After dried under vacuum at 50 °C for 48 h, the resin $PVBSO_2-Bs$ was obtained. Elemental analysis (%): S, 12.44.

Under the protection of nitrogen gas, 6.35 g of $PVBSO_2-Bs$ (ca. 12.32 mmol $phSO_3-$) resin were swollen sufficiently in 80 mL DMF in a three-neck flask for more than 2 h, and then 4.49 g (ca. 47.71 mmol) of AP and 2.20 g of K_2CO_3 (ca. 15.82 mmol) powder were added. With magnetic stirring, the mixture was reacted for 24 h at 120 °C. Then, the polymeric beads $PVBSO_2$-AP were filtered off and washed with dilute hydrochloric acid, dilute sodium hydroxide, distilled water, ethanol, acetone, and finally with methanol. The product $PVBSO_2$-AP was transferred to Soxhlet's extraction apparatus for reflux-extraction in 95 % ethanol for 10 h and then was dried under vacuum at 50 °C over 48 h. Elementary analysis: N, 1.633; S, 11.24.

2.3. Effect of pH on Adsorption. The effect of pH on the adsorption of Hg(II) was studied by adding 50.0 mg of silica-gel adsorbents to 1 mL of 0.1 mol·L^{-1} Hg(II) and 19 mL of buffer solution at different pH values in 100 mL Erlenmeyer flask. This mixture was mechanically shaken for 24 h at 25 °C to attain equilibrium. Then a certain volume of the solutions was separated from the adsorbents, and the residual concentration of Hg(II) was detected by means of AAS. The adsorption amount was calculated according to eq 1.

$$Q = \frac{(C_0 - C)V}{W} \tag{1}$$

where Q is the adsorption amount, mmol·g^{-1}; C_0 and C, the initial and final concentrations of metal ions in solution, mmol·mL^{-1}; V, the volume, mL; W, the dry weight of resin, g.

2.4. Kinetics Adsorption. In kinetics experiment, 100 mg of resin was added to 40 mL of 5 mmol·L^{-1} Hg(II) solution (pH 5.0). The mixture was shaken continuously at room temperature. At predetermined intervals, aliquots of 2 mL solution were withdrawn for analysis, and the concentration of metal ion was determined by atomic absorption spectrometry.

2.5. Isothermal Adsorption. The isothermal adsorption was investigated also by batch studies. A typical procedure is: a series of 50 mL test tubes were employed. Each test tube was filled with 20 mL of Hg(II) solution (pH 5.0) with varying concentrations. A known amount of resin (about 50 mg) was added into each test tube and agitated intermittently at 25 °C for the desired time periods, up to a maximum of about 12 h. The adsorption capacities were calculated also by using eq 1, where C is the equilibrium concentration of Hg(II) in solution.

2.6. Adsorption Selectivity. Selective separation of Hg(II) from binary mixtures with Ni(II), Zn(II), or Pb(II) was studied. A portion of 50 mg of resin (PVBSO-AP or $PVBSO_2$-AP) was placed in a 50 mL conical flask, then 2 mL of 0.1 mol·L^{-1} of Hg(II), 2 mL of 0.1 mol·L^{-1} Ni(II), Zn(II), or Pb(II), and 16 mL of buffer solution with pH 5.0 was added in turn. The mixture was shaken for 24 h at 25 °C. The mixture was filtered off, and the concentrations of the Hg(II) and coexistence metal ion were determined by atomic absorption spectrometry. The above-mentioned adsorption experiments were repeated three times. The adsorption capacities of Hg(II) and coexistence metal ion were calculated according to eq 1.

2.7. Regeneration of Resin. To assess the reusability of the resin, consecutive adsorption−desorption cycles were repeated three times by using the same resin. The solution of 5 % thiourea in 0.1 mol·L^{-1} HNO_3 was employed as the desorption medium based on our previous work.[10] The resin adsorbed Hg(II) was placed in this medium and stirred for 2 h at room temperature (a primary experimental showed that the Hg(II) adsorbed on resin was almost desorbed completely when the contact time of resin adsorbed Hg(II) with this medium was about 50 min). The final concentration of Hg(II) in the aqueous phase was determined by using AAS.

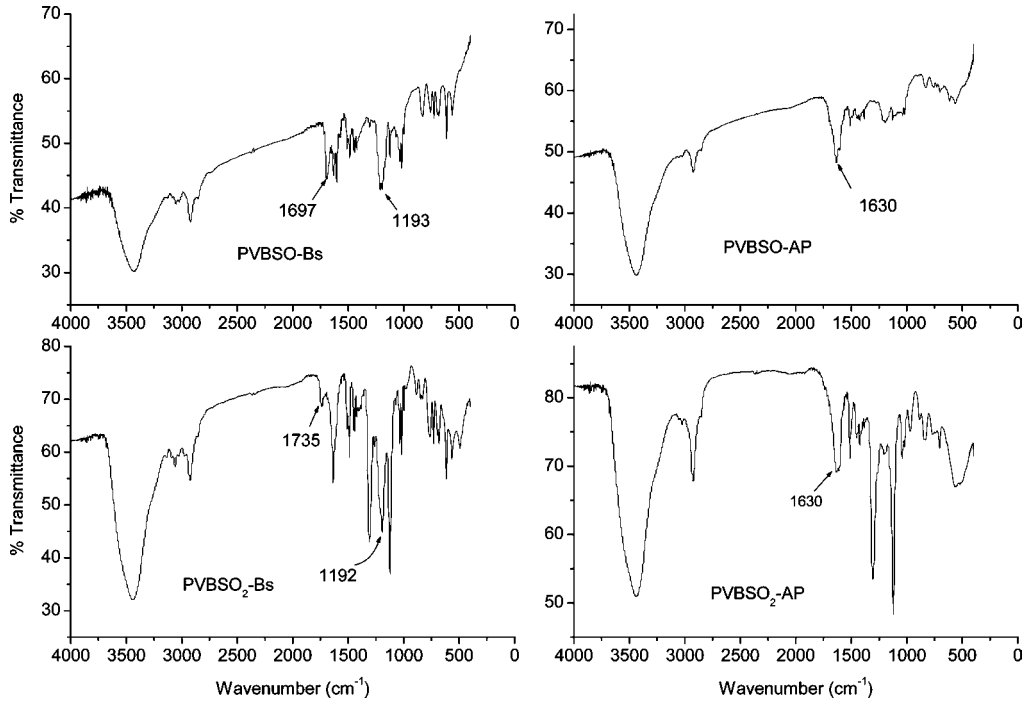

Figure 1. FTIR of PVBSO-Bs, $PVBSO_2$-Bs, PVBSO-AP, and $PVBSO_2$-AP.

3. Results and Discussion

3.1. Infrared Spectra and Elemental Analysis Characterization. The infrared spectra of the intermediates and PVBSO-AP and $PVBSO_2$-AP are shown in Figure 1. Under the present conditions, it is difficult to employ the IR method for confirming the existence of pyridyl ring in the resins PVBSO-AP and $PVBSO_2$-AP because its characteristic absorption peaks appeared around 1630 cm^{-1} are normally overlapped with those of benzene rings. So, in this study, the substitute reaction of amino pyridine with benzenesulfonal was demonstrated by monitoring the change of characteristic IR absorption of benzenesulfonal. The structure of the PVBSO-Bs was confirmed by the presence of new absorption bands at (1194 and 1697) cm^{-1}, which are designated as the stretching vibrations of O═S═O and the skeletal vibrations of benzene ring of benzenesulfonyl, respectively.[25] These bands weakened or disappeared in the infrared spectrum of PVBSO-AP indicating that AP had been introduced into the polymeric matrix. Similarly to PVBSO-Bs, the characteristic peak of O═S═O and the skeletal vibrations of benzene ring of benzenesulfonyl appeared at (1192 and 1735) cm^{-1}, respectively, in the curve of $PVBSO_2$-Bs, indicating that esterification reaction occurred and benzenesulfonyl groups have been introduced successfully to the structure of $PVBSO_2$-Bs. The successful introduction of AP into polymeric matrix can be corroborated by the disappearance of the characteristic absorption peaks of the above two absorption peaks.

According to the elemental analysis of nitrogen, the contents of AP in the PVBSO-AP and $PVBSO_2$-AP resins can be calculated to be (0.69 and 0.58) $mmol \cdot g^{-1}$ resin, which are much lower than their theoretical values of (2.15 and 2.21) $mmol \cdot g^{-1}$ resin. From this fact, it is clear that part of benzenesulfonate were still unreacted in the reaction of amino pyridine substitute for benzenesulfonal.

3.2. SEM Observations. To observe the surface morphology of PVBSO-AP and $PVBSO_2$-AP resins and their intermediates, scanning electron micrographs of the gold-coated samples were taken with a SEM, and the images are shown in Figure 2. It can be observed that the pore spaces on the surfaces of PVBSO-Bs and $PVBSO_2$-Bs increased comparing with the corresponding precursors PVBSO and $PVBSO_2$ resins because of the introduction of the benzene sulfonate group. After the reaction of PVBSO-Bs and $PVBSO_2$-Bs with AP, as observed from Figure 2, the surfaces of PVBSO-AP and $PVBSO_2$-AP beads became rougher and the pores distributed more abundantly than those of PVBSO-Bs and $PVBSO_2$-Bs beads, implying that the porous structures of polymer beads were still maintained after substitute reactions. These increases of pore amount can be interpreted as that pores which collapsed before the reaction reopened after the polar group AP were introduced into the polymeric matrix. The existence of rough surface and abundant pores would provide convenient diffusion channels for metal ions into the interior of PVBSO-AP and $PVBSO_2$-AP resins when they were used in adsorption of metal ions in aqueous solution. Also it should be noticed that the surface morphology of PVBSO-AP resin is different from that of $PVBSO_2$-AP resin, which is probably resulted from the differences in steric structure between the −SO− and $-SO_2-$.

3.3. Porous Structure Analysis. In general, the porous structures of porous materials can be characterized through the nitrogen adsorption−desorption isotherms. According to IUPAC classification, pores within porous materials can be divided into micropores (width less than 2 nm), mesopores (width between (2 and 50) nm), and macropores (width greater than 50 nm). It can be seen from Figure 3 that there was almost no nitrogen adsorbed at lower P/P_0 (by the mechanism of micropore filling), indicating that there were no micropores in both resins. A steep increase in nitrogen volume adsorbed at higher P/P_0 (by the mechanism of capillary condensation) suggested a quite large contribution in mesopore and macropore range in the both resins. In the entire region of relative pressure, the nitrogen volume adsorbed by PVBSO-AP was smaller than that by $PVBSO_2$-AP, indicating a lower porosity for PVBSO-AP, and it was consistent with the result obtained by SEM. It should be noticed that both the resins showed isotherms of type IV with inflection points around $P/P_0 = 0.9$ and the hysteresis loops exhibited almost the same form, meaning that the pore shapes of the resins were similar, that is, the pores had not been destroyed significantly during the reactions. Figure 4 shows the BJH

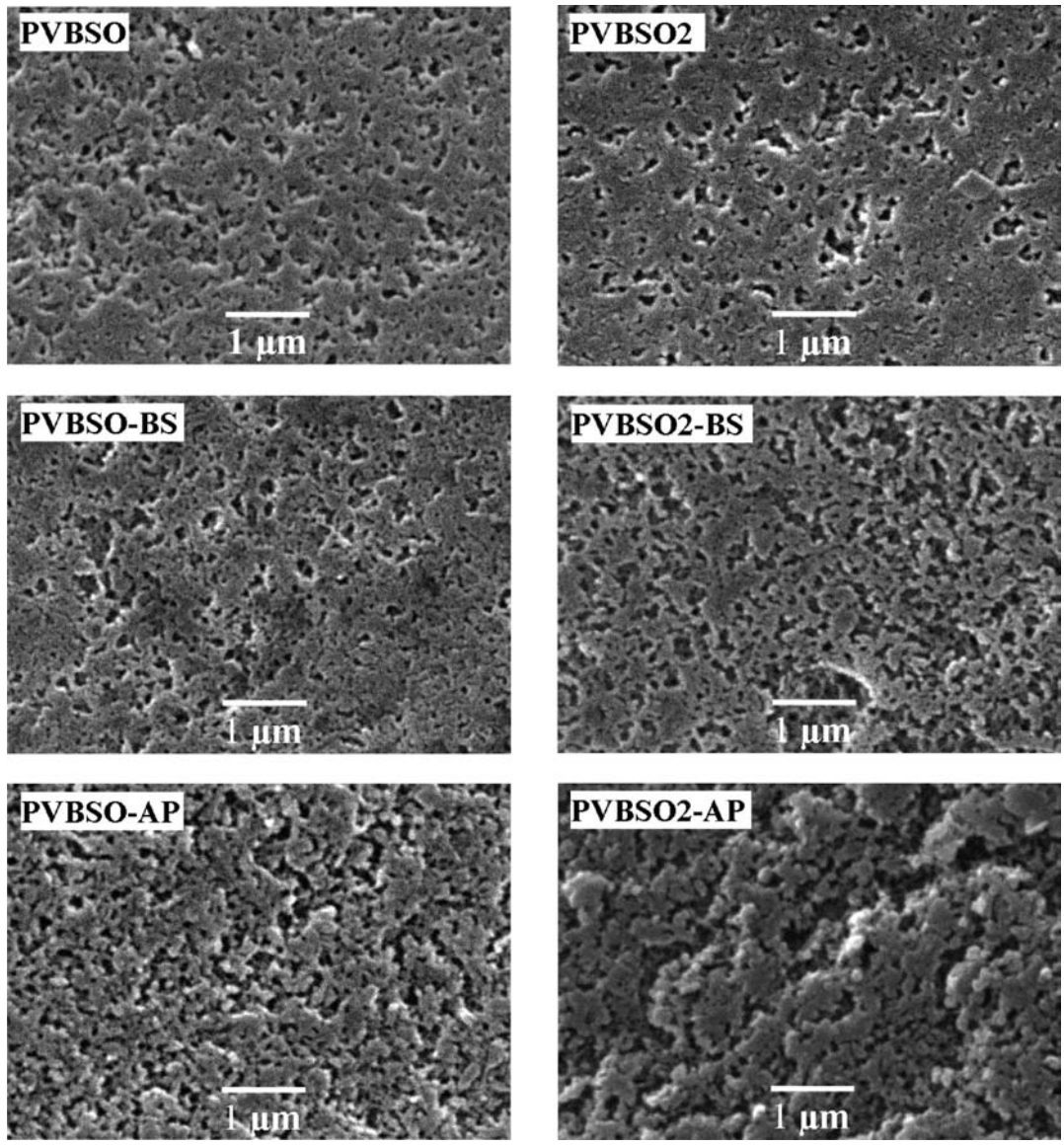

Figure 2. SEM images of surface of PVBSO-AP, $PVBSO_2$-AP, and their precursors.

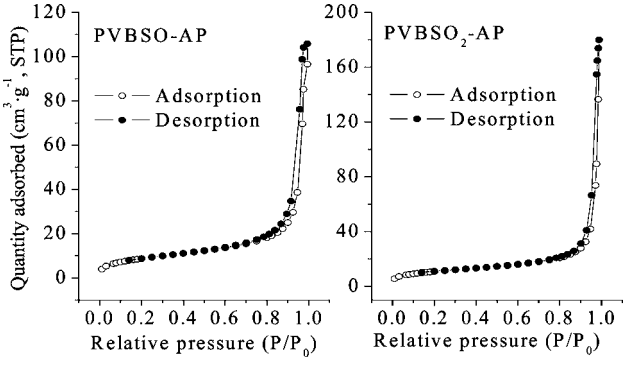

Figure 3. Nitrogen adsorption−desorption isotherms of PVBSO-AP and $PVBSO_2$-AP resins.

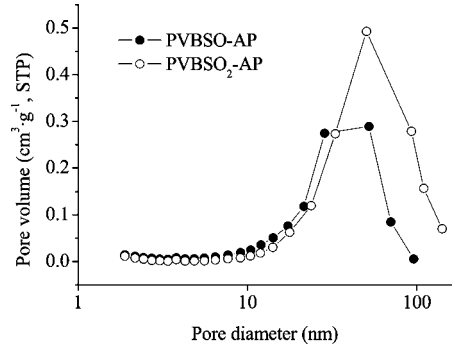

Figure 4. BJH desorption pore size distributions of PVBSO-AP and $PVBSO_2$-AP resins.

adsorption pore size distributions of the resins. As illustrated in Figure 4, the pores ranging from (10 to 100) nm and (10 to 145) nm were dominant for PVBSO-AP and $PVBSO_2$-AP resins, respectively. Also it can be seen that the volumes of the pores between (30 to 90) nm for PVBSO-AP were smaller than those for $PVBSO_2$-AP, which was probably because that the larger pores were stuffed due to the higher content of AP in PVBSO-AP resin than in $PVBSO_2$-AP resin. The porous structure parameters of the two resins derived from the basis of the nitrogen adsorption data are summarized in Table 1. As shown in Table 1, the values of BET surface area, BJH desorption average pore diameter, and BJH desorption cumulative volume of pores for $PVBSO_2$-AP were all larger than those for PVBSO-AP.

3.4. Effect of pH on Adsorption. It is well-known that solution pH is an important parameter affecting adsorption of

Table 1. Porous Structure Parameters of PVBSO-AP and $PVBSO_2$-AP Resins

resins	BET surface area ($m^2 \cdot g^{-1}$)	BJH desorption average pore diameter (nm)	BJH desorption cumulative volume of pores ($m^3 \cdot g^{-1}$)[a]
PVBSO-AP	32.45	22.92	0.16
$PVBSO_2$-AP	39.08	37.61	0.27

[a] The total volume of pores between (1.7 and 300) nm diameter.

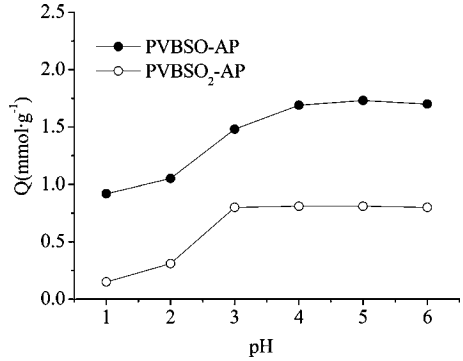

Figure 5. Effect of pH value on the Hg(II) adsorption on PVBSO-AP and $PVBSO_2$-AP resins.

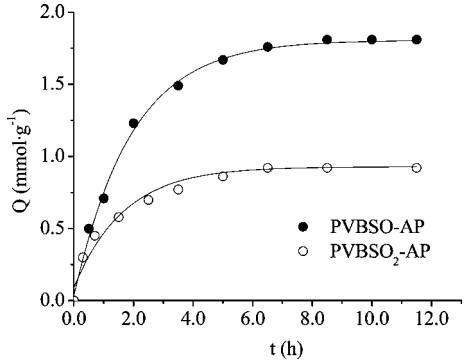

Figure 6. Kinetics of adsorption of Hg(II) on PVBSO-AP and $PVBSO_2$-AP resins at 25 °C (pH = 5.0).

metal ions on adsorbents, as it not only affects metal species in solution but also influences the surface properties of the adsorbents in terms of dissociation of functional groups and surface charges. So the effect of solution pH on the adsorption capacities of Hg(II) on PVBSO-AP and $PVBSO_2$-AP resins were investigated, and the results are shown in Figure 5. As can be seen from Figure 5, the solution pH had a significant effect on the adsorption, and the adsorption capacities increased with an increase in solution pH. The optimum pH ranges appeared at (4.0 to 5.0) for PVBSO-AP and (3.0 to 6.0) for $PVBSO_2$-AP resin, while the corresponding maximum adsorption capacities were (1.73 and 0.81) $mmol \cdot g^{-1}$, respectively. At lower pH, the positively charged hydrogen ions may compete with the Hg(II) for binding on the functional groups (amino or pyridyl group) on the adsorbents. Once the amine and pyridyl groups were protonated, the strong electrical repulsion prevented Hg(II) from contacting the surface of adsorbents, resulting in lower adsorption capacities. It should be noticed that the adsorption capacity of Hg(II) for PVBSO-AP resin was 0.92 $mmol \cdot g^{-1}$ and only 0.15 $mmol \cdot g^{-1}$ for $PVBSO_2$-AP resin under the same case of pH 1.0. This phenomenon can be interpreted as the stronger affinity of sulfoxide group in PVBSO-AP resin toward Hg(II) than that of sulfone group in $PVBSO_2$-AP resin. The results also show that the adsorption properties of the chelating resin containing sulfoxide and AP are clearly superior to the chelating resin containing sulfoxide and 3-aminopyridine.[24] The adsorption capacities of the resin containing sulfoxide and AP (1.73 $mmol \cdot g^{-1}$) are almost three times the resin containing sulfoxide and 3-aminopyridine (0.65 $mmol \cdot g^{-1}$). This finding shows the active synergetic effect between sulfoxide and AP on the adsorption for Hg(II). To obtain the maximum adsorption capacity, pH 5.0 was adopted in the kinetic and isotherm adsorption process.

3.5. Kinetic Adsorption. The uptake of Hg(II) over time at a pH of 5.0 is shown in Figure 6. It has been observed that the equilibrium time required for maximum removal of Hg(II) was (8.5 and 6.5) h for PVBSO-AP and $PVBSO_2$-AP resins, respectively. To ensure the adsorption balance completely, the adsorption time was fixed to 12 h in the subsequent adsorption experiments. It is clear that the adsorption capacity of Hg(II) on PVBSO-AP resin is higher than that on the $PVBSO_2$-AP one, which can be attributed to the following reasons: (1) PVBSO-AP resin possesses higher content of AP than $PVBSO_2$-AP; and (2) there exists synergetic effect between −SO− and AP in PVBSO-AP. In our previous work, we have demonstrated that the sulfur atom in −SO− can take part in coordinating with Hg(II), while the sulfur atom in $-SO_2-$ cannot.[25] Accordingly, the adsorption mechanism of Hg(II) on PAVBSO-AP and $PVBSO_2$-AP resins can be presumed as Scheme 2a,b.

The kinetic models were used to test the experimental data and thus elucidate the adsorption kinetic process.

The pseudofirst-order[26] and pseudosecond-order[27] equations were represented as:

$$\log(Q_0 - Q) = \log Q_0 - \frac{k_1}{2.303}t \qquad (2)$$

Scheme 2. Adsorption Mechanism of Hg(II) on PVBSO-AP and $PVBSO_2$-AP

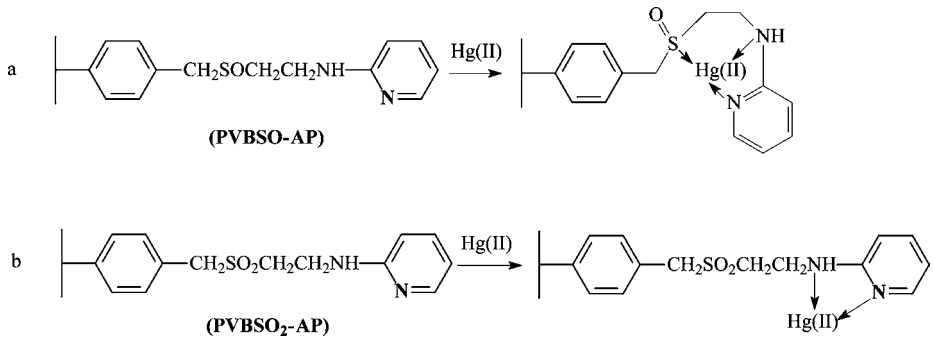

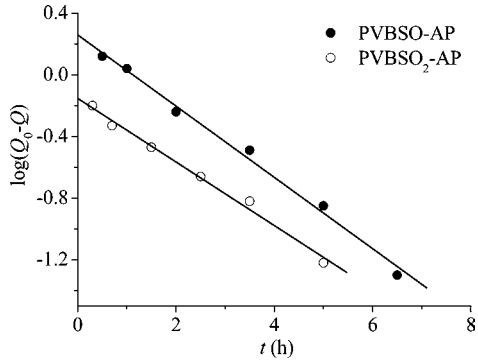

Figure 7. Pseudofirst-order kinetic plots for the adsorption of Hg(II) onto PVBSO-AP and $PVBSO_2$-AP.

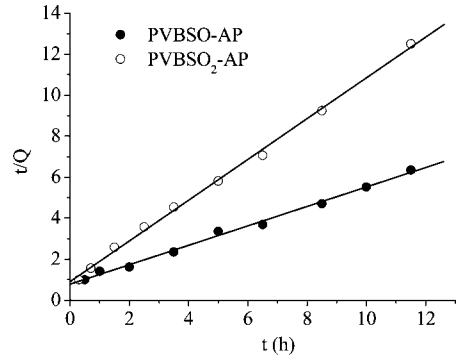

Figure 8. Pseudosecond-order kinetic plots for the adsorption of Hg(II) onto PVBSO-AP and $PVBSO_2$-AP.

$$\frac{t}{Q} = \frac{1}{k_2 Q_0^{\,2}} + \frac{t}{Q_0} \tag{3}$$

where k_1 (h^{-1}) is the pseudofirst-order adsorption rate constant (h^{-1}) of adsorption k_2 ($g \cdot mmol^{-1} \cdot h^{-1}$), the rate constant of pseudosecond-order adsorption rate constant, and Q_0 and Q ($mmol \cdot g^{-1}$) are the amounts of metal ion adsorbed at equilibrium and time t (h), respectively. The value of log ($Q_0 - Q$) was calculated from the experimental results and plotted against t (h) in Figure 7. The pseudosecond-order equation is tested by plotting t/Q against time (t) in Figure 8. The kinetic parameters (k_1, k_2, Q) and correlation coefficients (R_1^2, R_2^2) of Hg(II) ions were calculated and are listed in Table 2. As seen from Figure 8, the pseudosecond-order model fits the data very well, and the R_2^2 values were found to be 0.9950 and 0.9976 for PVBSO-AP and $PVBSO_2$-AP resins, respectively (Table 2). Although the plots of Hg(II) on PVBSO-AP show linearity, the calculated Q values (2.10 $mmol \cdot g^{-1}$) were not in agreement with the experimental Q values (1.81 $mmol \cdot g^{-1}$), suggesting that the adsorption of Hg(II) on PVBSO-AP does not follow pseudosecond-order kinetics. As can be seen from Table 2, the obtained R_1^2 value for PVBSO-AP was 0.9926. Moreover, the calculated Q values are in good agreement with experimental Q values. Hence, the adsorption kinetics could be well-approximated more favorably by the pseudofirst-order kinetic model for Hg(II) onto PVBSO-AP. Recently, a theoretical analysis of the pseudosecond-order model was reported.[28] According to this theoretical approach, when the initial concentration of solute is high, its adsorption kinetics fits better to the pseudofirst-order model and better to the pseudosecond-order for the low initial concentration. Thus, it is concluded that, for the adsorption system of Hg(II) on PVBSO-AP, the observed rate constant is a linear function of the initial concentration of solute; its slope and intercept are adsorption and desorption rate constants, respectively.

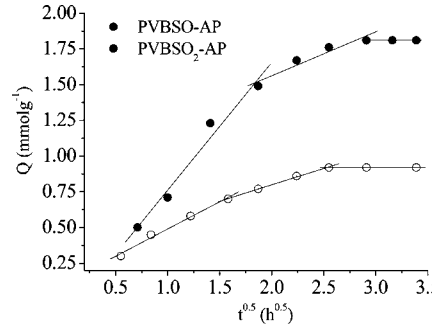

Figure 9. Intraparticle diffusion model plots for the adsorption of Hg(II) onto PVBSO-AP and $PVBSO_2$-AP.

The adsorption kinetic data was further tested as to whether the intraparticle diffusion model[29] can be described as

$$Q = k_{id} t^{0.5} \tag{4}$$

where k_{id} is the intraparticle diffusion rate constant, which can be obtained from the slope of the plot Q versus $t^{0.5}$. If the regression of Q versus $t^{0.5}$ is linear and passes through the origin, then intraparticle diffusion is the sole rate-limiting step.[30] As seen from Figure 9, the straight line did not pass through the origin, suggesting that intraparticle diffusion may not be the only rate-controlling step. The plots are shown in Figure 9, indicating multilinearity with three distinct phases. The initial curved portion relates to the external surface adsorption. The second linear portion is due to intraparticle or pore diffusion, and the final portion (plateau) is attributed to the equilibrium stage. The intercept of the plot provides an estimation of the thickness of the boundary layer, that is, the larger the intercept value, the greater the boundary layer effect is. The slope of second linear portion of the plot has been identified as intraparticle diffusion rate constant k_{id}.[31] The values of intercept and intraparticle rate diffusion constant (k_{id}) are given in Table 2. The slope of second linear portion of the plot of any resins is much lower compared to the first one, which is due to the lower adsorption rate in the intraparticle or pore diffusion.

3.6. Isothermal Adsorption. Langmuir, Freundlich, and Redlich−Peterson isotherms are the most commonly used isotherms for different adsorbent−adsorbate systems to explain solid−liquid adsorption systems.[32−34] LThe angmuir equation relates the coverage of molecules on a solid surface to concentration of a medium above the solid surface at a fixed temperature. The Langmuir model represents one of the theoretical treatments and suggests that uptake occurs

Table 2. Coefficients of Pseudofirst-Order and Pseudosecond-Order Kinetic Models and an Intraparticle Diffusion Model

		pseudofirst-order kinetics			pseudosecond-order kinetics			intraparticle diffusion	
resins	Q_0(exp) ($mmol \cdot g^{-1}$)	k_1(h^{-1})	Q_0 (cal) ($mmol \cdot g^{-1}$)	R_1^2	k_2($g \cdot mmol^{-1} \cdot h^{-1}$)	Q_0(cal) ($mmol \cdot g^{-1}$)	R_2^2	k_{id} ($mg \cdot g^{-1} \cdot h^{0.5}$)	R_{id}^2
PVBSO-AP	1.81	0.53	1.82	0.9926	0.29	2.10	0.9950	0.31	0.9654
$PVBSO_2$-AP	0.92	0.48	0.70	0.9917	1.10	1.00	0.9976	0.23	0.9987

on a homogeneous surface by monolayer sorption without interaction between adsorbed molecules.[35] Moreover, the Langmuir model served to estimate the maximum metal uptake values where they could not be reached in the experiments.[36] The Freundlich isotherm, an empirical equation, is capable of describing the adsorption of organic and inorganic compounds on a wide variety of adsorbents. The Freundlich model proposes an adsorption with a heterogeneous energetic distribution of active sites, accompanied by interactions between adsorbed molecules.[35] Redlich−Paterson is another empirical equation, designated as the "three-parameter equation," which is capable to represent adsorption equilibrium over a wide concentration range. Redlich and Paterson incorporated the characteristics of Langmuir and Freundlich isotherms into a single equation. Two limiting behaviors exist, that is, Langmuir form for g equal 1 and Henry's law form for g equal 0.[37]

The expression of the Langmuir, Freundlich, and Redlich−Peterson isotherms can be represented as:

$$Q = \frac{Q_0 bC}{1 + bC} \tag{5}$$

$$Q = k_F C^{1/n} \tag{6}$$

$$Q = \frac{AC}{1 + BC^g} \tag{7}$$

The linearized forms of Freundlich and Langmuir equations are:

$$\frac{C}{Q} = \frac{1}{bQ_0} + \frac{C}{Q_0} \tag{8}$$

$$\ln Q = \ln k_F + \frac{1}{n} \ln C \tag{9}$$

$$\ln\left(A\frac{C}{Q} - 1\right) = g \ln C + \ln B \tag{10}$$

where Q is the amount of metal adsorbed per unit weight of adsorbent at equilibrium (mmol·g^{-1}); C is the left-out solute concentration at equilibrium (mmol·L^{-1}); Q_0 is the Langmuir monolayer sorption capacity (mmol·g^{-1}); b is an empirical parameter related to equilibrium constant or energy of adsorption (L·mmol^{-1}); k_F is the Freundlich constant related to the bonding energy constant reflecting the affinity of the resin to Hg(II) (mmol·g^{-1})(L·g^{-1})^n; n is the Freundlich exponent related to adsorption intensity, respectively; A is the Redlich−Peterson isotherm constant,(L·g^{-1}); B is the Redlich−Peterson isotherm constant (L/mmol$^{1-(1/A)}$); and g is Redlich−Peterson isotherm exponent, which lies between 0 and 1.

In this study, the experimental data in Figure 10 were analyzed using linearized Langmuir, Freundlich, and Redlich−Peterson equations by plotting C/Q versus C, ln Q versus ln C, and ln(AC/Q − 1) versus ln C, respectively, and their nonlinear equations by plotting Q versus C. The calculated isotherm parameters and corresponding R^2 are shown in Table 3. From Table 3, it can be observed that the Langmuir isotherm model exhibited a good fit to the experimental adsorption data since the R^2 values for PVBSO-AP were 0.9919. These results showed that the Langmuir isotherm model fitted the results quite well,

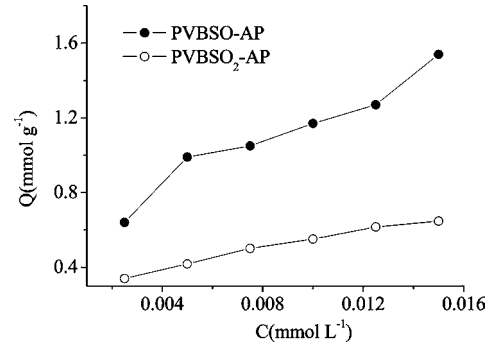

Figure 10. Adsorption isotherms of Hg(II) on PVBSO-AP and $PVBSO_2$-AP resins at 25 °C (pH = 5.0).

Table 3. Isotherm Parameters Obtained by Using the Linear Method

equations	parameters	PVBSO-AP	$PVBSO_2$-AP
linear Langmuir	Q_0	2.01	0.82
	b	267.30	168.24
	R^2	0.9919	0.9965
linear Freundlich	k_F	9.16	3.04
	n	2.28	2.71
	R^2	0.9567	0.9955
linear Redlich−Peterson	A	434.94	4000
	B	256.85	4365
	g	0.99	0.94
	R^2	0.9893	0.9849

suggesting that the surface of PVBSO-AP is homogeneous. Each binding site accepts only one Hg(II), and the adsorbed Hg(II) are organized as a monolayer. All sites are energetically equivalent, and there is no interaction between adsorbed Hg(II). The Freundlich isotherm equation describes the adsorption of solute from liquid to solid surface and assumes that the stronger binding sites are occupied first and that the binding strength decreases with the increasing degree of site occupation.[36] The results of present study indicate that the Freundlich model does not fit the experimental data since the R^2 values were 0.9567 for PVBSO-AP but fit the experimental data for $PVBSO_2$-AP (R^2 = 0.9947). Similarly, the Redlich−Peterson linear model is unable to fit the experimental data as low correlation coefficients.

The best correlation of experimental data with the linear Langmuir isotherm suggests the monolayer coverage and chemisorption of Hg(II) onto PVBSO-AP resins. The n values are between 2 and 5 for PVBSO-AP, indicating the adsorption processes are carried out easily.[37]

From Table 3, it is observed that the maximum monolayer adsorption capacity of Hg(II) adsorbed on PVBSO-AP and $PVBSO_2$-AP resins are found to be (2.01 and 0.82) mmol·g^{-1} (calculated based on linearized Langmuir equation), respectively. The reasons resulting in the difference of the two resins in maximum adsorption capacity include: (1) the sulfoxide group in PVBSO-AP resin exhibited greater affinity than sulfone group in $PVBSO_2$-AP resin to Hg(II), the B and k_F values of the former higher than that of the latter (see Table 3), which represent the affinity of resin to metal ions, demonstrated this deduction; and (2) the content of amino pyridine of PVBSO-AP resin is higher than that of $PVBSO_2$-AP.

3.7. Adsorption Selectivity. A series of binary metal ions systems were chosen as representatives to investigate the selective adsorption of Hg(II) on PVBSO-AP and $PVBSO_2$-AP resins. The results are presented in Table 4. Obviously, both PVBSO-AP and $PVBSO_2$-AP resins could selectively adsorb Hg(II) when it coexisted with Ni(II), Zn(II), and Pb(II),

Table 4. Selectivity of Adsorption of Hg(II) on PVBSO-AP and $PVBSO_2$-AP Resins in Binary Ion Systems

resin	systems	metal ions	adsorption capacity ($mmol \cdot g^{-1}$)	selective coefficient[a]
PVBSO-AP	Hg(II)−Ni(II)	Hg(II)	2.27	$\alpha_{Hg/Ni} = \infty$
		Ni(II)	0	
	Hg(II)−Zn(II)	Hg(II)	2.16	$\alpha_{Hg/Zn} = 9.39$
		Zn(II)	0.23	
	Hg(II)−Pb(II)	Hg(II)	2.73	$\alpha_{Hg/Pb} = \infty$
		Pb(II)	0	
$PVBSO_2$-AP	Hg(II)−Ni(II)	Hg(II)	1.20	$\alpha_{Hg/Ni} = \infty$
		Ni(II)	0	
	Hg(II)−Zn(II)	Hg(II)	1.48	$\alpha_{Hg/Zn} = \infty$
		Zn(II)	0	
	Hg(II)−Pb(II)	Hg(II)	1.26	$\alpha_{Hg/Pb} = \infty$
		Pb(II)	0	

[a] The selective coefficients were the ratio of adsorption capacities of metal ions in binary mixture.

Table 5. Repeated Adsorption of Hg(II) Ions by PVBSO-AP and $PVBSO_2$-AP (Adsorption Conditions: Initial Concentration $5 \cdot 10^{-3}$ M, pH 5.0, 25 °C)

	adsorption of the resins ($mmol \cdot g^{-1}$)	
reuse times	PVBSO-AP	$PVBSO_2$-AP
1	2.11	0.50
2	2.01	0.56
3	1.98	0.51

respectively, which indicated that PVBSO-AP and $PVBSO_2$-AP resins could be probably used in extracting and separating Hg(II) from a multi-ionic system. However, PVBSO-AP has obvious superiority due to higher adsorption capacities for Hg(II).

3.8. Regeneration of Resin. A solution of 5 % thiourea in 0.1 $mol \cdot L^{-1}$ HNO_3 was chosen to use as eluent to desorb Hg(II) from PVBSO-AP and $PVBSO_2$-AP resins and to regenerate them. The results of three adsorption−desorption cycles are shown in Table 5. The data in Table 5 suggest that the PVBSO-AP resin with higher adsorption capacities is especially suitable for repeating use for three cycles of adsorption−desorption without considerable changes of adsorption capacity.

4. Conclusions

(1) FTIR and elemental analysis demonstrated that porous cross-linked polystyrene modified with 2-amino-pyridine via sulfoxide/sulfone-containing spacer arm chelating resins, PVBSO-AP and $PVBSO_2$-AP, were synthesized successfully.

(2) SEM and porous structure analysis proved that porous structures of polymer beads were still maintained after substitute reactions. The values for BET surface area, BJH desorption average pore diameter, and BJH desorption cumulative volume of pores for $PVBSO_2$-AP were all larger than those for PVBSO-AP.

(3) The kinetics of adsorption of Hg(II) on the two resins showed that the adsorption process followed the pseudosecond-order model for PVBSO-AP and the pseudofirst-order model for $PVBSO_2$-AP. The linear Langmuir model is the best-fitted isotherm to describe the adsorption of Hg(II) on the PVBSO-AP resin.

(4) Both PVBSO-AP and $PVBSO_2$-AP can selectively adsorb Hg(II) from binary ion systems in the presence of the coexistent ions Ni(II), Zn(II), and Pb(II), but PVBSO-AP has obvious superiority because of higher adsorption capacities for Hg(II).

(5) PVBSO-AP resin with higher adsorption capacities is suitable for repeating the use for three cycles of adsorption−desorption without considerable change of adsorption capacities.

Literature Cited

(1) Meng, L. Z.; Gong, S. L.; Yin, Y. H.; Chen, Y. Y.; Wang, Y. W. Network crown ether resin with pendent sulfur ether group: Preparation, thermodegradation, and adsorption behavior. *J. Appl. Polym. Sci.* **2003**, *87*, 1445–1451.

(2) Sreedhar, M. K.; Anirudhan, T. S. Preparation of an adsorbent by graft polymerization of acrylamide onto coconut husk for mercury(II) removal from aqueous solution and chloralkali industry wastewater. *J. Appl. Polym. Sci.* **2000**, *75*, 1261–1269.

(3) Vieira, E. F. S.; Cestari, A. R.; Santos, E. B.; Dias, F. S. Interaction of Ag(I), Hg(II), and Cu(II) with 1,2-ethanedithiol immobilized on chitosan: Thermochemical data from isothermal calorimetry. *J. Colloid Interface Sci.* **2005**, *289*, 42–47.

(4) Atia, A. A.; Donia, A. M.; Elwakeel, K. Z. Selective separation of mercury (II) using a synthetic resin containing amine and mercaptan as chelating groups. *React. Funct. Polym.* **2005**, *65*, 267–275.

(5) Say, R.; Garipcan, B.; Emir, S.; Patir, S.; Denizli, A. Preparation and characterization of the newly synthesized metal-complexing-ligand n-methacryloylhistidine having phema beads for heavy metal removal from aqueous solutions. *Macromol. Mater. Eng.* **2002**, *287*, 539–545.

(6) Bernabé, L.; Rivas, S.; Pooley, A.; Aceitón, E.; Geckeler, K. E. Synthesis, characterization, and properties of a selective adsorbent to mercury(II) ions. *J. Appl. Polym. Sci.* **2002**, *85*, 2559–2563.

(7) Navarro, R. R.; Sumi, K.; Fuij, N.; Matsumura, M. Mercury removal from wastewater using porous cellulose carrier modified with polyethyleneimine. *Water. Res.* **1996**, *30*, 2488–2494.

(8) Bozena, N. K.; Orota, J. B.; Andrzej, W. T.; Wieslaw, A. Influence of the structure of chelating resins with guanidyl groups on gold sorption. *React. Funct. Polym.* **1999**, *42*, 213–222.

(9) Ridvan, S.; Tuncel, A.; Denizli, A. Adsorption of Ni^{2+} from aqueous solutions by novel polyethyleneimine-attached poly(*p*-chloromethylstyrene) beads. *J. Appl. Polym. Sci.* **2002**, *83*, 2467–2473.

(10) Qu, R. J.; Sun, C. M.; Chen, J.; Chen, H.; Wang, C. H.; Ji, C. N.; Xu, L. L. Preparation and coordination with Hg(II) of sulfur- and 2-aminopyridine-containing chelating resin. *Polym. Eng. Sci.* **2007**, *47*, 721–727.

(11) Mondal, B. C.; Das, A. K. Determination of mercury species with a resin functionalized with a 1,2-bis(*o*-aminophenylthio)ethane moiety. *Anal. Chim. Acta* **2003**, *477*, 73–80.

(12) Jeon, C.; Par, K. H. Adsorption and desorption characteristics of mercury(II) ions using aminated chitosan bead. *Water. Res.* **2005**, *39*, 3938–3944.

(13) Grote, M.; Schumacher, U. Bipolar ion-exchange resins based on functional acidic tetrazolium groups − their synthesis, structure and properties. *React. Funct. Polym.* **1997**, *35*, 179–196.

(14) Sartore, L.; Penco, M.; Bignotti, F.; Peroni, I.; Gil, M. H.; Ramos, M. A.; Damore, A. Grafting of selected presynthesized macromonomers onto various dispersions of silica particles. *J. Appl. Polym. Sci.* **2002**, *85*, 1287–1296.

(15) Yavuz, E.; Senkal, B. F.; Bicak, N. Poly(acrylamide) grafts on spherical polyvinyl pyridine resin for removal of mercury from aqueous solutions. *React. Funct. Polym.* **2005**, *65*, 121–125.

(16) Baba, Y.; Ohe, K.; Kawasaki, Y.; Kolev, S. D. Adsorption of mercury(II) from hydrochloric acid solutions on glycidylmethacrylate-divinylbenzene microspheres containing amino groups. *React. Funct. Polym.* **2006**, *66*, 1158–1164.

(17) Donia, A. M.; Atia, A. A.; Heniesh, A. M. Efficient removal of Hg(II) using magnetic chelating resin derived from copolymerization of bisthiourea/thiourea/glutaraldehyde. *Sep. Purif. Technol.* **2008**, *60*, 46–53.

(18) Donia, A. M.; Atia, A. A.; Elwakeel, K. Z. Selective separation of mercury(II) using magnetic chitosan resin modified with Schiff's base derived from thiourea and glutaraldehyde. *J. Hazard. Mater.* **2008**, *151*, 372–379.

(19) Ji, C. N.; Qu, R. J.; Wang, C. H.; Chen, H.; Sun, C. M.; Xu, Q.; Sun, Y. Z.; Wei, C. A chelating resin with bis[2-(2-benzothiazolylthioethyl)sulfoxide]: Synthesis, characterization and properties for the removal of trace heavy metal ion in water samples. *Talanta* **2007**, *73*, 195–201.

(20) Qu, R. J.; Sun, C. M.; Ji, C. N.; Wang, C. H.; Zhao, Z. G.; Yu, D. S. Synthesis and adsorption properties of macroporous cross-linked polystyrene that contains an immobilizing 2,5-dimercapto-1,3,4-thiodiazole with tetraethylene glycol spacers. *Polym. Eng. Sci.* **2005**, *45*, 1515–1521.

(21) Qu, R. J.; Wang, C. H.; Ji, C. N.; Sun, C. M.; Sun, X. R.; Cheng, G. X. Preparation, characterization, and metal binding behavior of novel chelating resins containing sulfur and polyamine. *J. Appl. Polym. Sci.* **2005**, *95*, 1558–1565.

(22) Qu, R. J.; Sun, C. M.; Ji, C. N.; Xu, Q.; Wang, C. H.; Cheng, G. X. The sorption mechanism of Au(III) on sulfur-containing chelating resin poly[4-vinylbenzyl(2-hydroxyethyl) sulfide]. *Eur. Polym. J.* **2006**, *42*, 254–258.
(23) Qu, R. J.; Sun, C. M.; Wang, C. H.; Ji, C. N.; Sun, Y. Z.; Guan, L. X.; Yu, M. Y.; Cheng, G. X. Preparation and metal binding behavior of poly(4-vinylbenzyl 2-hydroxyethyl) sulfoxide and sulfone. *Eur. Polym. J.* **2005**, *41*, 1525–1530.
(24) Ji, C. N.; Qu, R. J.; Wang, C. H.; Sun, C. M.; Chen, H.; Sun, Y. Z.; Liu, J. Synthesis, Characterization, and properties for Hg^{2+} of new chelating resin containing sulfoxide and 3-aminopyridine. *J. Appl. Polym. Sci.* **2008**, *108*, 2144–2149.
(25) Xie, J. Y. *The Application of Infrared Spectra in Organic Chemistry and Medicine Chemistry*; Science Press: Beijing, 1987.
(26) Razvigorova, M.; Budinova, T.; Petrov, N.; Minkova, V. Purification of water by activated carbons from apricot stones, lignites and anthracite. *Water. Res.* **1998**, *32*, 2315–2139.
(27) Ho, Y. S.; McKay, G. Pseudo-second order model for sorption processes. *Process Biochem.* **1999**, *34*, 451–465.
(28) Azizian, S. Kinetic models of sorption: a theoretical analysis. *J. Colloid Interface Sci.* **2004**, *276*, 47–52.
(29) Weber, W. J.; Morris, J. C. Kinetics of adsorption of carbon from solutions. *J. Sanit. Eng. Div., Am. Soc. Civ. Eng.* **1963**, *89*, 31–63.
(30) Ozcan, A.; Ozcan, A. S. Adsorption of Acid Red 57 from aqueous solutions onto surfactant-modified sepiolite. *J. Hazard. Mater.* **2005**, *125*, 252–259.
(31) Ramesh, A.; Hasegawa, H.; Sugimoto, W.; Maki, T.; Ueda, K. Adsorption of gold(III), platinum(IV) and palladium(II) onto glycine modified crosslinked chitosan resin. *Bioresour. Technol.* **2008**, *99*, 3801–3809.
(32) Ho, Y. S.; Chiu, W. T.; Hsu, C. S.; Huang, C. T. Sorption of lead ions from aqueous solution using tree fern as a sorbent. *Hydrometallurgy* **2004**, *73*, 55–61.
(33) Ho, Y. S. Removal of copper ions from aqueous solution by tree fern. *Water. Res.* **2003**, *37*, 2323–2330.
(34) Ho, Y. S. Selection of optimum sorption isotherm. *Carbon* **2004**, *42*, 2115–2116.
(35) Sari, A.; Mendil, D.; Tuzen, M.; Soylak, M. Biosorption of palladium(II) from aqueous solution by moss (Racomitrium lanuginosum) biomass: Equilibrium, kinetic and thermodynamic studies. *J. Hazard. Mater.* **2009**, *162*, 874–879.
(36) Khambhaty, Y.; Mody, K.; Basha, S.; Jha, B. Kinetics, equilibrium and thermodynamic studies on biosorption of hexavalent chromium by dead fungal biomass of marine *Aspergillus niger*. *Chem. Eng. J.* **2009**, *145*, 489–495.
(37) Febrianto, J.; Kosasiha, A. N.; Sunarso, J.; Ju, Y. H.; Indraswati, N.; Ismadji, S. Equilibrium and kinetic studies in adsorption of heavy metals using biosorbent: A summary of recent studies. *J. Hazard. Mater.* **2009**, *162*, 616–645.

Received for review May 14, 2010. Accepted September 4, 2010. The authors are grateful for the financial support by the National Natural Science Foundation of China (No. 51073075), the Natural Science Foundation of Shandong Province (No. ZR2009FM075, 2008BS04011, Y2007B19), the Nature Science Foundation of Ludong University (No. 08-CXA001, 032912, 042920, LY20072902), and the Educational Project for Postgraduate of Ludong University (No. YD05001, Ycx0612).

JE100506D